EasyChair Preprint

№ 3976

Strain Effects on Electronic and Optical Properties of Monolayer Mo-Dichalcogenides

Thanh Van Vuong, Thuy Dung Nguyen, Bach Le Xuan, Van Nguyen Duy, Loi Giap Van, Bao Hoang Van, Truong Do Wang and Hung Nguyen Tuan

July 30, 2020

Strain effects on electronic and optical properties of monolayer Mo-dichalcogenides

Vuong Van Thanh[1], Nguyen Thuy Dung[1], Le Xuan Bach[1], Nguyen Duy Van[1], Giap Van Loi[1], Hoang Van Bao[1], Do Van Truong[2] and Nguyen Tuan Hung[3]

[1]Department of Design of Machinery and Robot, School of Mechanical Engineering, Hanoi University of Science and Technology, Hanoi, Vietnam
thanh.vuongvan@hust.edu.vn
[2]Department of Mechatronics, School of Mechanical Engineering, Hanoi University of Science and Technology, Hanoi, Vietnam
[3]Frontier Research Institute for Interdisciplinary Sciences, Tohoku University, Sendai 980-8578, Japan

Abstract. Using first-principles calculations, we investigate mechanical, electronic, and optical properties of monolayer MoX_2 (X = S, Se, and Te) under biaxial tensile strain. The obtained results indicate that MoS_2 shows the highest stiffness and ideal strength among MoX_2. In unstrain cases, MoS_2 is an indirect-gap semiconductor, while $MoSe_2$ and $MoTe_2$ are direct-gap semiconductors. The energy band-gaps of MoX_2 decrease with the increasing of the biaxial tensile strain. Furthermore, the biaxial tensile strain effectively modulates the optical absorption of MoX_2. Our calculated results provide useful information for applications in nano-electromechanical, optoelectronic, and photocatalytic devices based on MoX_2.

Keywords: Transition metal dichalcogenides**,** ideal strength, density functional theory, optical absorption.

1. Introduction

Two-dimensional (2D) transition metal dichalcogenides (TMDs) have been increasing attention for nanoelectronic, optoelectronic and photocatalytic devices because of their remarkable properties [1], such as an indirect-to-direct band-gap transition [2], multi-excitons [3] and high carrier mobility [4]. Recently, monolayer MoS_2 has been successfully fabricated through chemical vapor deposition [5]. Li*et et al.*[6] showed that the monolayer MoS_2 exhibits an out-of-plane soft-mode phonon instability under biaxial tension and uniaxial tension along the armchair direction at the ideal strain. Hong *et al*. [7] indicated that the electronic properties of MoS_2 are very sensitive to the lattice structure. Therefore, by applying a strain to deform the lattice structure, the electronic and optical properties of the TMDs can be tuned.

In recent years, many studies have been focused on the strain engineering of the TMDs to investigate the effect of strain on the electronic properties of TMDs [8]. Based on the first-principles calculations, Yue *et al*. [9] indicated that monolayer MoS_2 has a direct to indirect transition at a strain ~ 1% and a semiconductor-to-metal transition at a strain ~10%. In another theoretical study, Scalise *et al*. [10] also indicated that MoS_2 shows a direct to indirect transition at a tensile strain of up to ~ 2%. The bandgaps are reduced to almost zero at the tensile strains about 10% and 11% for WSe_2 and WTe_2, respectively [11]. The effect of strain on the optical properties of the 2D TMDs has also been widely investigated [11, 12]. On the other hand, the biaxial strain can easy to access by experiment with atomic force microscope-based technique [13]. Therefore, a systematic investigation of biaxial tensile

strain on the mechanical, electronic, and optical properties of the 2D MoX_2 (X= S, Se, and Te) monolayers is essential for nano-electromechanical and optoelectronic applications.
In the paper, we investigate the mechanical, electronic, and optical properties of the monolayer MoX_2 as a function of the biaxial tensile strain using the first-principles calculation. We show that MoS_2 is the strongest in the MoX_2 compounds with Young's modulus about 197 GPa and the ideal strength of about 24.48 GPa. Besides, we also discuss the effect of the strain on the electronic and optical properties of MoX_2.

2. Computational methods

First-principles calculations have been performed within the density-functional theory (DFT) by using Quantum ESPRESSO package [14]. An energy cut-off of 60 Ry is used for the wave function. The exchange-correlation energy is evaluated by general gradient approximation with the Perdew–Burke–Ernzerhof (PBE) function [15]. The **k**-point grids in the Brillouin zone are set by 16 x 16 x 1 for all models with the Monkhorst–Pack method [16].

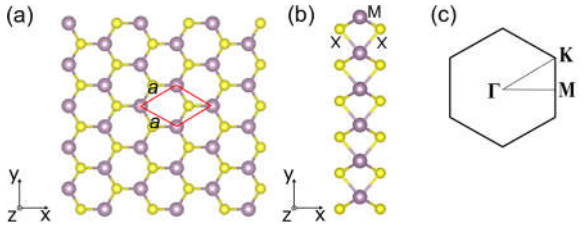

Fig. 1. Top view (a) and side view (b) of monolayer MoX_2. (c) First Brillouin zone of monolayer MoX_2 with high symmetry points (Γ, K, M).

In Fig. 1, we show the atomic structure of MoX_2, in which the periodic boundary condition is applied, and a vacuum space of 30 Å in the direction perpendicular to the monolayer (*z*-direction) is set to avoid virtual interactions between layers. To obtain optimized structures of the monolayer MoX_2, the atomic positions and cell vectors are relaxed by using the Broyden–Fletcher–Goldfarb–Shanno (BFGS) minimization method [17] until all the Hellmann–Feynman forces and all components of the stress are less than 0.0005 Ry/a.u. and 0.05 GPa, respectively.
Themo-pw code [18] is used to calculate the elastic constants C_{ij} of the monolayer MoX_2. Since the values of C_{ij} are related to the equivalent volume of the unit cell, the calculated C_{ij} must be rescaled by h/d_0, where h is the length of the cell along *z*-axis and d_0 is the effective layer thickness of the monolayer MX_2 (d_0 = 6.145 Å) [19], we assume that the effective layer thickness does not change under the strain. The Young's modulus, Y, and the Poisson's ratio, υ, of the monolayer materials can be obtained as follows [19, 20].

$$Y = \frac{C_{11}^2 - C_{22}^2}{C_{11}}, \text{ and } \upsilon = \frac{C_{12}}{C_{11}} \tag{1}$$

To investigate the ideal strength σ_{bia} and ideal strain ε_{bia} (ε_{bia} is the strain at the maximum stress) of the monolayer MoX_2 under the strain, a biaxial tensile strain is applied to the structures by elongating the cell in biaxial direction with an increment of 0.02 of the tensile strain until the structure is broken. Here, the dimensionless tensile strain is defined by $\varepsilon = (L - L_0)/ L_0$, where L and L_0 are the length of the unit cell for the strained and unstrained structures, respectively.
To obtain the optical properties of the monolayer MoX_2 under the biaxial tensile strain, we calculated the optical absorption coefficient $\alpha(\omega)$ using the following equation [21].

$$\alpha(\omega) = \frac{\sqrt{2}\omega}{c}[\sqrt{\varepsilon_1^2(\omega) + \varepsilon_2^2(\omega)} - \varepsilon_1(\omega)]^{1/2} \tag{2}$$

where $\varepsilon_1(\omega)$ and $\varepsilon_2(\omega)$ are real and imaginary parts of the dielectric function, respectively, c is the speed of light in the vacuum and ω is the angular frequency of light.

3. Results and discussion

In Table 1, we show the optimized lattice constants of the monolayer MoX_2, in which the lattice constants of MoX_2 increase with increasing of the atomic number of X, Z_X ($Z_S<Z_{Se}<Z_{Te}$), atoms. The obtained results are consistent with other calculations [19,22], indicating that the present calculations are reasonable and reliable. The values of the elastic constants C_{ij}, Young's modulus Y, and Poisson's ratio ν of MoX_2 are listed in Table 1. It is found that the Young's modulus of MoS_2 is the largest value, followed by $MoSe_2$ and $MoTe_2$, indicating that MoS_2 is the stiffest with Y=197 GPa. We note that the lattice constant of MoS_2 (3.19Å) is smaller than that of $MoSe_2$ (3.31Å) and $MoTe_2$ (3.55Å), respectively.

Table 1. Lattice constant a_0 (Å), elastic constants C_{ij} (GPa), Young's modulus Y (GPa), Poisson's ratio ν, ideal strength σ_{bia}(GPa) and ideal strain (ε_{bia}) of the MoX_2.

Materials	a	C_{11}	C_{12}	C_{66}	Y	ν	σ_{bia}	ε_{bia}
MoS_2	3.19	207	42	83	197	0.2	24.48	0.196
$MoSe_2$	3.31	173	32	71	167	0.18	19.91	0.196
$MoTe_2$	3.55	129	41	44	116	0.32	14.2	0.221

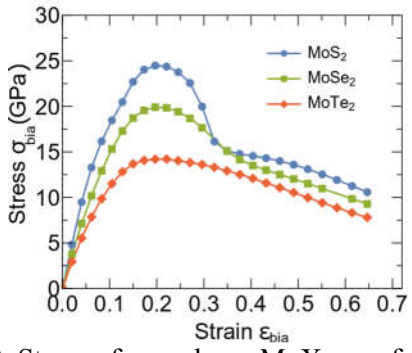

Fig. 2. Stress of monolayer MoX_2 as a function of biaxial tensile strain.

In Fig. 2, we show the stress-strain curves of MoX_2 under the biaxial strain. The ideal strengths of MoX_2 are arranged as follows: MoS_2> $MoSe_2$> $MoTe_2$. The ideal strength of MoS_2 is 24.48 GPa, and the corresponding ideal strain is 0.196, which is in an excellent agreement with the previous theoretical study (23.8 GPa) [8] and experimental data (22± 4 GPa) [17]. The ideal strength of MoS_2 and $MoSe_2$ is larger than that of phosphorene (18 GPa) [23]. The ideal strength and ideal strain of all monolayers MoX_2 are listed in Table 1.

In Figs. 3 (a), (b), and (c), we show the band structures of the monolayer MoX_2 at three biaxial strains (ε_{bia}= 0, 0.04, and 0.08), respectively. As shown in Fig. 3, the band structures of MoX_2 are significantly modified by the biaxial strain. At unstrain case, ε_{bia}= 0, MoS_2 is an indirect-gap semiconductor with an energy band-gap of 1.58 eV, while $MoSe_2$ and $MoTe_2$ are direct-gap semiconductors with the bottom of the conduction band (CBM) and the top of the valence band (VBM) at the K point in the Brillouin zone. At ε_{bia}= 0.04, $MoSe_2$ becomes an indirect-gap semiconductor with bandgap of 0.89 eV. On the other hand, at ε_{bia} = 0.04, $MoTe_2$ is still a direct-gap semiconductor with band gap of 0.81 eV. These results suggest that not only bandgap but also direct-indirect transition of MoX_2 is tuned by applying biaxial tensile strain. As shown in Fig. 4, the bandgaps of MoX_2 are plotted as a function of the biaxial strain, in which the bandgap of MoX_2 decreases with increasing the biaxial tensile strain. This trend is also observed in previous studies for the 2D Janus TMDs [21].

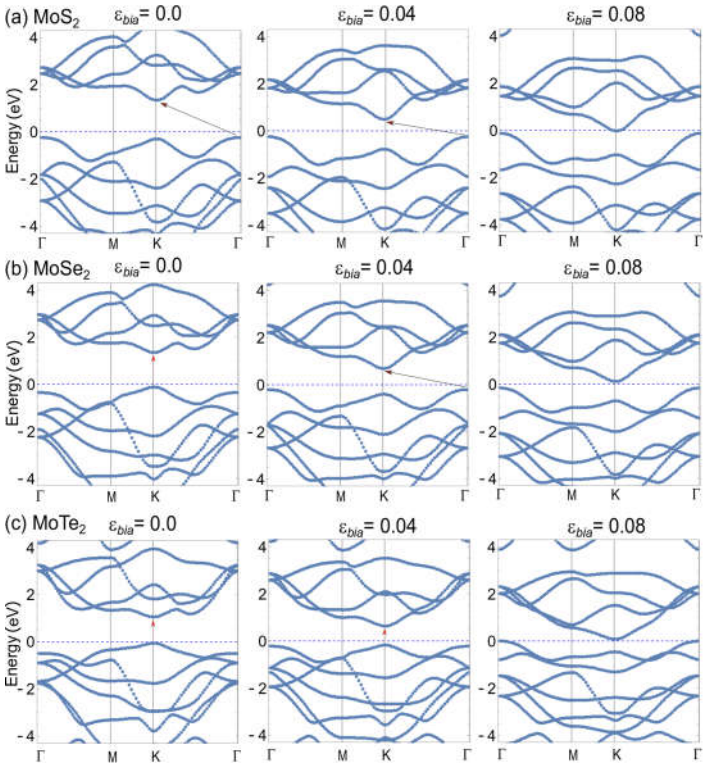

Fig. 3. Energy band structures of MoX_2 as a function of biaxial tensile strain.

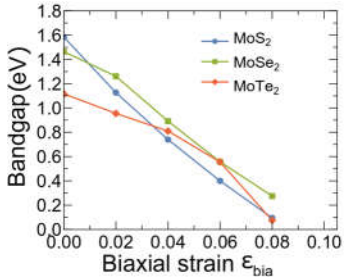

Fig. 4. Energy bandgaps of monolayer MoX_2 as a function of biaxial tensile strain.

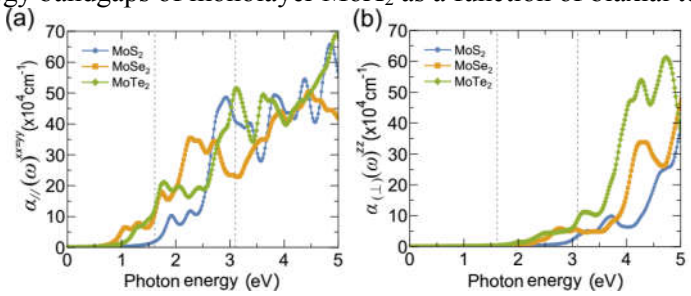

Fig. 5. Optical absorption of MoX_2 along the (a) in-plane ($\alpha_{//}(\omega)$) and (b) out-of-plane ($\alpha_{\perp}(\omega)$) at the unstrain case (ε_{bia}= 0). The dash lines denote the range of visible light from 1.61 eV to 3.10 eV.

In Figs. 5 (a) and (b), we show the optical absorption $\alpha(\omega)$ of MoX_2 at the unstrain (ε_{bia}= 0) in the energy range from 0 to 5 eV, in which $\alpha(\omega)$ is calculated by Eq. (2). We find that $\alpha(\omega)$ exhibits a strong anisotropy along the polarization directions ($\alpha_{//}(\omega)^{xx} = \alpha_{//}(\omega)^{yy} > \alpha_{\perp}(\omega)^{zz}$). In the visible-light region, $\alpha(\omega)$ of the MoX_2 along the in-plane ($\alpha_{//}(\omega)^{xx} = \alpha_{//}(\omega)^{yy}$) direction is much larger than that of

the out-of-plane ($\alpha_{\perp}(\omega)$) direction with one order of magnitude, which is consistent with the previous first-principles study for the Janus TMDs [21]. For the in-plane direction, MoX_2 exhibits strong absorption when the photon energy is more than 2eV, as shown in Fig. 5 (a). The optical absorption of MoX_2 reaches around 10 x 10^4 cm^{-1} to 50 x 10^4 cm^{-1} at the visible-light region, which is higher than that of Janus TMDs [21] (15 x 10^4 cm^{-1} - 30 x 10^4 cm^{-1}). For the out-of-plane, $MoTe_2$ has the largest value of 10 x 10^4 cm^{-1} at 3.1 eV, as illustrated in Fig. 5 (b).

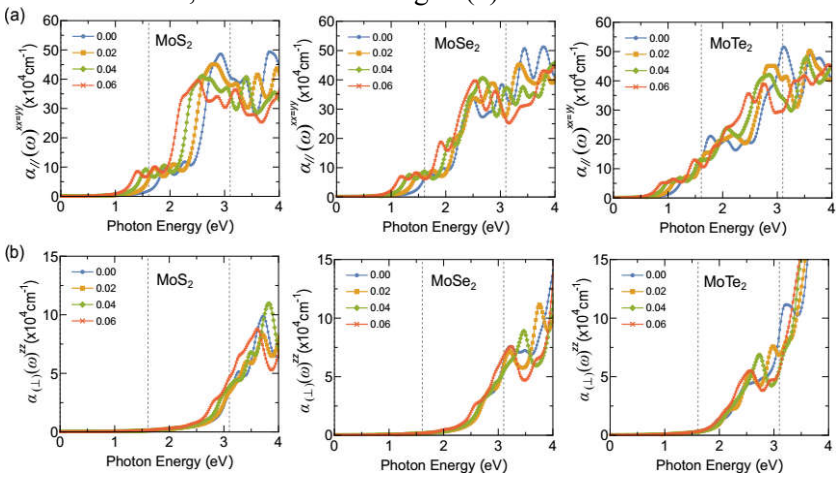

Fig. 6. Optical absorption of monolayer MoX_2 along the (a) in-plane ($\alpha_{//}(\omega)$) and (b) out-of-plane ($\alpha_{\perp}(\omega)$) as a function of photo energy for several biaxial tensile strains (ε_{bia} = 0.0; 0.02; 0.04 and 0.06). The dash lines denote the range of visible light from 1.61 eV to 3.10 eV.

In Figs. 6 (a) and (b), we show the optical absorption $\alpha(\omega)$ of MoX_2 for several biaxial tensile strain along the in-plane ($\alpha_{//}(\omega)$) and out-of-plane ($\alpha_{\perp}(\omega)$) directions, respectively. Under the biaxial tensile strain, $\alpha_{//}(\omega)$ is much enhanced at around 2.5 eV, while $\alpha_{\perp}(\omega)$ does not show a significant change. As shown in Fig. 6 (a), for MoS_2, at the photon energy of 2.3 eV, $\alpha_{//}(\omega)$ increases from 10 x 10^4 cm^{-1} to 40 x 10^4 cm^{-1}. From the results obtained above, we note that the optical spectra, as well as electronic properties of the monolayer MoX_2 are quite sensitive to biaxial tensile strain, which is an important characteristic for their applications in the optoelectronic and electro-mechanical devices. Interestingly, among the MoX_2 compounds, MoS_2 shows not only the highest stiffness but also good optical properties under the biaxial tensile strain.

4. Conclusions

In summary, we have investigated the mechanical, electronic, and optical properties of the monolayer MoX_2 under the biaxial tensile strains by using the first-principles calculations. We find that MoS_2 is the strongest in the mentioned MoX_2 compounds. The band structures of MoX_2 can be modulated by using the external biaxial strain. The bandgap of MoX_2 decreases with increasing biaxial strain. Furthermore, the optical absorption coefficient of MoX_2 is enhanced by applying the biaxial tensile strain. In particular, the in-plane optical absorption of MoS_2 is increased by four times at photon energy of 2.5 eV and the biaxial strain of 0.02. The obtained results are useful for the design and fabricating of electronic and optical devices based on the monolayer MoX_2.

References

1. Kam, K. K., & Parkinson, B. A. Detailed photocurrent spectroscopy of the semiconducting group VIB transition metal dichalcogenides. The Journal of Physical Chemistry, 86(4), 463-467 (1982).
2. Mak, K. F., Lee, C., Hone, J., Shan, J., & Heinz, T. F. Atomically thin MoS_2: a new direct-gap semiconductor. Physical review letters, 105(13), 136805, (2010).
3. Mak, K. F., He, K., Lee, C., Lee, G. H., Hone, J., Heinz, T. F., & Shan, J. Tightly bound trions in monolayer MoS_2. Nature materials, 12(3), 207-211, (2013).

4. Baugher, B. W., Churchill, H. O., Yang, Y., & Jarillo-Herrero, P. Intrinsic electronic transport properties of high-quality monolayer and bilayer MoS_2. Nano letters, 13(9), 4212-4216, (2013).
5. Kim, D., Sun, D., Lu, W., Cheng, Z., Zhu, Y., Le, D., & Bartels, L. Toward the growth of an aligned single-layer MoS_2 film. Langmuir, 27(18), 11650-11653, (2011).
6. Li, T. Ideal strength and phonon instability in single-layer MoS_2. Physical Review B, 85(23), 235407 (2012).
7. Hong, J., Hu, Z., Probert, M., Li, K., Lv, D., Yang, X., ... & Zhang, J. Exploring atomic defects in molybdenum disulphide monolayers. Nature communications, 6(1), 1-8, . (2015)
8. Chen, X., & Wang, G. Tuning the hydrogen evolution activity of MS_2 (M= Mo or Nb) monolayers by strain engineering. Physical Chemistry Chemical Physics, 18(14), 9388-9395, (2016).
9. Yue, Q., Kang, J., Shao, Z., Zhang, X., ... & Li, J. Mechanical and electronic properties of monolayer MoS_2 under elastic strain. Physics Letters A, 376(12-13), 1166-1170, (2012).
10. Scalise, E., Houssa, M., ...& Stesmans, A. Strain-induced semiconductor to metal transition in the two-dimensional honeycomb structure of MoS_2. Nano Research, 5(1), 43-48, (2012).
11. Liu, J., Liu, H., Wang, J., Sheng, H., Tang, G., Zhang, J., & Bai, D. Optical and electronic properties of dichalcogenides WX_2 (X= S, Se, and Te) monolayers under biaxial strain. Physica B: Condensed Matter, 568, 18-24, (2019).
12. Feierabend, M., Morlet, A., Berghäuser, G., & Malic, E. Impact of strain on the optical fingerprint of monolayer transition-metal dichalcogenides. Physical Review B, 96(4), 045425, (2017).
13. Bertolazzi, S., Brivio, J., & Kis, A. Stretching and breaking of ultrathin MoS_2. ACS nano, 5(12), 9703-9709, (2011).
14. Giannozzi, P., Baroni, S., Bonini, N., Calandra, M., Car, R., Cavazzoni, C., ... & Dal Corso, A. QUANTUM ESPRESSO: a modular and open-source software project for quantum simulations of materials. Journal of physics: Condensed matter, 21(39), 395502, (2009).
15. Perdew, J. P., Burke, K., & Ernzerhof, M. Generalized gradient approximation made simple. Physical review letters, 77(18), 3865, (1996).
16. Monkhorst, H. J., & Pack, J. D. Special points for Brillouin-zone integrations. Physical review B, 13(12), 5188, (1976).
17. Broyden, C. G. The convergence of a class of double-rank minimization algorithms 1. general considerations. IMA Journal of Applied Mathematics, 6(1), 76-90, (1970).
18. Dal Corso, A. Elastic constants of beryllium: a first-principles investigation. Journal of Physics: Condensed Matter, 28(7), 075401, (2016).
19. Van Thanh, V., & Hung, N. T. Charge-induced electromechanical actuation of Mo-and W-dichalcogenide monolayers. RSC advances, 8(67), 38667-38672, (2018).
20. Van Thanh, V., & Hung, N. T. Charge-induced electromechanical actuation of two-dimensional hexagonal and pentagonal materials. Physical Chemistry Chemical Physics, 21(40), 22377-22384, (2019).
21. Van Thanh, V., Van, N. D., Saito, R., & Hung, N. T. First-principles study of mechanical, electronic and optical properties of Janus structure in transition metal dichalcogenides. Applied Surface Science, 146730, (2020).
22. Ding, Y., Wang, Y., Ni, J., Shi, L., Shi, S., & Tang, W. First principles study of structural, vibrational and electronic properties of graphene-like MX_2 (M= Mo, Nb, W, Ta; X= S, Se, Te) monolayers. Physica B: Condensed Matter, 406(11), 2254-2260 (2011).
23. Wei, Q., & Peng, X. Superior mechanical flexibility of phosphorene and few-layer black phosphorus. Applied Physics Letters, 104(25), 251915, (2014).